Particuology 91 (2024) 260–267

Contents lists available at ScienceDirect

Particuology

journal homepage: www.elsevier.com/locate/partic

Impact of the spindle number on the material transport and mixing during planetary roller melt granulation

Tom Lang, Jens Bartsch*

Laboratory of Solids Process Engineering, Department of Biochemical and Chemical Engineering, TU Dortmund University, 44227, Dortmund, Germany

ARTICLE INFO

Article history:
Received 1 December 2023
Received in revised form
28 February 2024
Accepted 29 February 2024
Available online 1 April 2024

Keywords:
Continuous manufacturing
Melt granulation
Planetary roller granulator
Quality-by-Design
Residence time
Material mixing

ABSTRACT

In comparison to the established twin-screw machines, the application of a planetary roller granulator for continuous operation of melt granulation is a promising alternative based on the unique process concept. An initial study focused on the material transport during processing as a key driver for the overall performance. Hereby, the impact of direct process parameters on the residence time distribution was the main objective.

These investigations are complemented in this study by considering the free processing volume, which is defined by the number of planetary spindles applied within a module. The impact on the processing conditions is evaluated with respect to the process setting in terms of feed rate and rotation speed.

The results highlight the potential of altering the underlying transport function in planetary roller melt granulation (PRMG) via the investigated direct process and equipment parameters. The impact of the feed rate is lower in comparison, while a higher rotation speed as well as a higher free processing volume promote material mixing. Moreover, a normalization of the determined residence time distribution (RTD) model data was feasible with respect to the process settings and the number of applied planetary spindles in the processing zone. This demonstrates the key role of the free processing volume in the fundamental mechanisms of material transport and mixing during PRMG.

1. Introduction

Granulation is a central unit operation of powder processing, which is usually applied to improve the bulk properties with respect to handling (Serno, Kleinebudde, & Knop, 2007). Here, two major trends of current research are the establishment of technologies for continuous manufacturing as well as for melt granulation. In the first case, this paradigm shift of production especially in the pharmaceutical industry aims for a reduction of the product quality fluctuations (Kleinebudde, Khinast, & Rantanen, 2017). In the second case, a main driver is a solvent-free processing, which e.g. enables the handling of materials prawn to hydrolytic effects (Weatherley, Mu, Thompson, Sheskey, & O'Donnell, 2013). Lately, in addition to the standard co-rotating twin-screw systems for continuous melt granulation (Forster, Dippold, & Chiang, 2021; Pradhan et al., 2022; Sekyi, Kelly, & Rahmanian, 2023; van de Steene et al., 2023b), the use of a planetary roller granulator has been introduced (Nesges, Lang, Birr, Thommes, & Bartsch, 2023) as a promising alternative. The characteristics of this method refer to the unique process concept based on the orbital motion of planetary spindles in a static roller cylinder driven by a rotating central spindle. At the same time, the inner and outer limit of the process zone are heated independently of each other (Fig. 1). For an initial study, the spindle number was kept constant in order to focus on the impact of direct process parameters on the material transport and mixing (Lang, Bramböck, Thommes, & Bartsch, 2023). Hereby, the residence time distribution (RTD) served as basis for the experimental characterization and was complemented by the application of a corresponding model.

This approach fits a trend of the last decade as the RTD has been a central element of research focus for various processes in powder technology including blending (Gyürkés et al., 2020; Razavi et al., 2023; Tian et al., 2022), extrusion (Ellwanger, Pernice, Karbstein, & Emin, 2023; Gottschalk et al., 2022; Wesholowski, Podhaisky, & Thommes, 2019), granulation (Plath, Korte, Sivanesapillai, & Weinhart, 2021; Tomita, Takeuchi, Natsuyama, & Takeuchi, 2021), tableting (Forgber et al., 2022; Peterwitz, Gerling, & Schembecker,

* Corresponding author.
E-mail address: jens.bartsch@tu-dortmund.de (J. Bartsch).

https://doi.org/10.1016/j.partic.2024.02.010

Nomenclature

A_{free}	Free area of the planetary roller processing cross section, m^2
A_{RC}	Inner cross-sectional area of the roller cylinder, m^2
c_0	Signal strength of initial tracer concentration, * (unit dependent on measurement method)
d_{CS}	Diameter of central spindle, mm
d_{PS}	Diameter of planetary spindle, mm
d_{RC}	Diameter of roller cylinder, mm
E	Residence time density function, s^{-1}
F	Cumulative residence time function
f_s	Correction factor regarding contacted surface per spindle rotation
h_{cs}	Pitch of central spindle, mm
k_0	Scaling parameter, s^{-1}
l_{cs}	Length of central spindle, mm
$\dot{m}$	Feed rate of material pre-mix, kg h^{-1}
n	Rotation speed of central spindle, min^{-1}
N_{PS}	Number of planetary spindles in a module
SFL	Specific feed load
t	Time, s
t_{50}	Median of residence time distribution, s
$\bar{t}$	Mean residence time, s
t_{dead}	Process dead time, s
t^*_{dead}	Dimensionless process dead time
$t^*_{dead,norm.}$	Normalized, dimensionless process dead time
t_{mix}	Process mixing time, s
t^*_{mix}	Dimensionless mixing time
$t^*_{mix,norm.}$	Normalized, dimensionless mixing time
ρ_{bulk}	Untapped bulk density of material pre-mix, kg m^{-3}
σ	Transport function width, s
σ^*	Dimensionless width of transport function
$\sigma^*_{norm.}$	Normalized, dimensionless width of transport function
τ	Hydrodynamic mean residence time, s

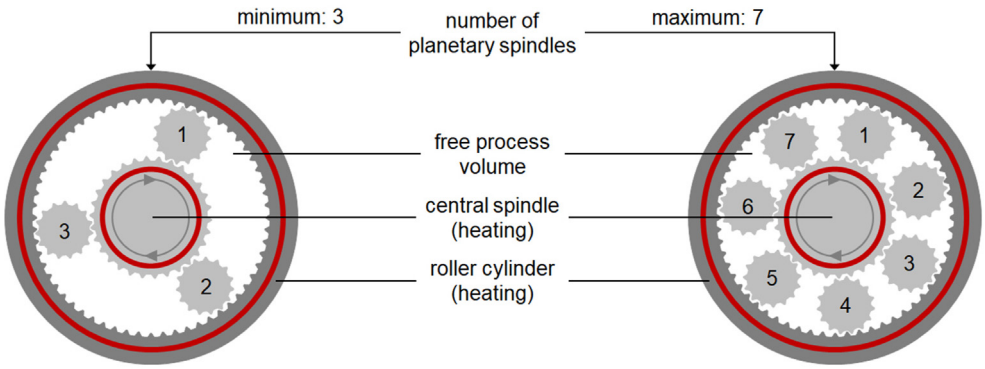

Fig. 1. Schematic cross-sectional area of the planetary roller granulator for a minimum (left) and maximum (right) number of planetary spindles within a module for the lab-scale machine size. Adapted and expanded from (Lang et al., 2023).

2022; Puckhaber, Eichler, Kwade, & Finke, 2020) and coating (Rosas et al., 2023; Sibanc, Turk, & Dreu, 2018). In this context, the residence time distribution is a measure to reflect the dynamics of a single process unit or a whole process line (Karttunen et al., 2019; Pauli, Kleinebudde, & Krumme, 2020) and consequently a suitable design tool for the continuous manufacturing (Bhalode et al., 2021; ICH, 2023; Karttunen et al., 2019).

With respect to process design, the characteristic parameters of the residence time distribution offer manifold information on the process itself, e.g. the available time for solution of a drug in a molten matrix carrier for the production of an amorphous solid dispersion (Van Renterghem et al., 2017; Winck, Daalmann, Berghaus, & Thommes, 2022) or the maximum thermal stress applied to the material with respect to degradation effects (Aldhafeeri, Alotaibi, & Barry, 2022; Liu & Zhang, 2023; Yaghini & den Doelder, 2023). Of course, the physical interpretation of the RTD characteristics depends on the connected process. For melt granulation, the relevance of the RTD refers to the fundamental rate processes of granulation (van de Steene et al., 2023a). These were elaborated by Iveson et al. (Iveson, Litster, Hapgood, & Ennis, 2001). The phase of *nucleation and growth* depends on the contacting of the molten binder with the material that shall be granulated. Hereby, the on-set of the RTD as the first detected tracer signal is crucial representing the minimal available time for melting and/or distributing the binder. The phase of *agglomeration and attrition* depends on the interaction of particles. Therefore, the mixing extent symbolized by the width of the RTD is a controlling factor in this respect. At the same time, the *attrition and breakage* of granules during processing relies on the applied mechanical stress and the duration of this. Therefore, the maximum hereby is reflected by the off-set of the residence time.

The aim of this study is to expand the approach of the previous one (Lang et al., 2023) on characterizing the processing conditions during planetary roller melt granulation (PRMG). Hereby, the main objective is the impact on the residence time by the variation of the planetary spindle number within the processing section. This aspect of the module configuration next to the spindle type defines directly the free processing volume and thereby the material transport and mixing mechanisms with respect to the general process concept. These aspects are reflected by a RTD model, which is fit to the experimental data, and the corresponding characteristic parameters.

2. Materials and methods

2.1. Planetary roller melt granulation

For the melt granulation experiments, a model compound (Lactose monohydrate, Lactose 310, Foremost Farms USA, Baraboo, USA) at 90 wt% and a meltable binder (Hydroxypropylcellulose, Klucel EXF Pharm, Ashland Inc., Covington, USA) at 10 wt% was blended a priori (RRM ELTE 650, J. Engelsmann AG, Lugwigshafen, Germany) and then fed with a gravimetric system (DDW-*M*-DS(R) 28, Brabender GmbH & Co. KG, Duisburg, Germany) into a lab-scale planetary roller granulator (PWE 30, Entex Rust & Mitschke GmbH, Bochum, Germany). The processing section was build-up of a single module with an effective length of 222 mm. The corresponding diameter of the mechanical parts were 35.4 mm for the roller cylinder, 17.7 mm for the central spindle and 8.8 mm for the planetary spindles. At the end, the granular product was discharged virtually pressure-free through an open orifice. During processing, the temperature for both heating systems was constantly set to 150 °C. A schematic of the set-up is given in (Lang et al., 2023).

2.2. Experimental design space

Main experimental focus was the variation of the free processing volume. Therefore, the planetary spindle number in the module was altered. The minimum was three due to mechanical stability with a free cross-sectional area of 553 mm^2 and the maximum was seven for the lab-scale granulator with a free cross-sectional area of 308 mm^2 (Fig. 1). A number of five planetary spindles was also applied as mean value in-between with a free cross-sectional area of 430 mm^2. However, in all cases the module was only equipped with the standard spindle type (SSP).

For the residence time determination, an experimental design space valid for all three investigated configurations was defined according to Nesges et al. (2023). The directly varied process parameters included the feed rate ($\dot{m}$) in the range of 0.3–1.2 kg h^{-1} and the rotation speed (n) from 60 to 240 min^{-1}. Each on four equidistant levels. Only exception is the combination of lowest rotation speed and highest feed rate for the maximum spindle number, which could not be executed due to the motor torque limit. The process parameters variations are condensed in the specific feed load (SFL) as a surrogate (Eq. (1)).

$$SFL = \frac{\dot{m}}{n\ \rho_{bulk}\ h_{cs}\ A_{free}} \tag{1}$$

This indirect measure adapted from twin-screw processes (Kohlgrüber, 2016; Wesholowski, Hoppe, Nickel, Muehlenfeld, & Thommes, 2019) to PRMG (Lang et al., 2023) symbolizes the generated mass flow per one revolution of the central spindle in comparison to the feed rate. Therefore, the SFL considers also the bulk density (ρ_{bulk}), the free cross-sectional area (A_{free}) for a module configuration and the pitch length of the central spindle (h_{cs}), which equals the diameter of the central spindle due to the 45° toothing of the mechanical parts.

2.3. Characterization of the residence time

In general, the residence time distribution is a probability function describing the exit time (t) of a single integrity after entering a process represented by the density function (E) or the cumulative time function (F). Both are mathematically linked, as one is the integral of the other with a limit value of 1 (Eq. (2)). Characteristic parameters are the median (t_{50}) of the distribution or the mean residence time ($\bar{t}$) as the first momentum of the residence time density function (Eq. (3) and (4)). Both parameters are equal for the special case of a normal distribution, but differ for any other type.

$$F\ (t \to \infty) = \int_0^{t\to\infty} E(t)dt = 1 \tag{2}$$

$$\int_0^{t_{50}} E(t)dt = 0.5 \tag{3}$$

$$\bar{t} = \int_0^{t\to\infty} E(t)\ t dt \tag{4}$$

The residence time density distribution for the different direct process parameter sets and module configurations was experimentally determined with pulse-signal experiments. Hereby, E104 or Ponceau 4R (ExtruVis, MeltPrep GmbH, Graz, Austria) was used as marker at a ratio of 20.83 s^{-1} with respect to the feed rate. The response signal was measured at the material discharge via an online camera system (ExtruVis, MeltPrep GmbH, Graz, Austria). The suitability of this method has already been demonstrated for PRMG (Lang et al., 2023) and other processes (Forster, Dippold, Haser, Emanuele, & Meier, 2023; Wilms & Kleinebudde, 2021). Based on the experimental data, the RTD is further evaluated via the Two-Compartment-model (Reitz, Podhaisky, Ely, & Thommes, 2013). This model comprehends a process as the superimposition of an axial transport with ideal mixing in a continuous stirred tank reactor. The first function is represented by the dead time (t_{ds}) and the distribution width (σ), while the mixing time (t_{mix}) refers to the second function (Eq. (5)). In addition, the model considers a scaling parameter (k_0), while the integral function is represented by initial signal intensity (c_0). This parameter should equal 1, when the fitted data sets are pre-treated and normalized to derive the density distribution. When a concentration function is represented, c_0 refers to the initial marker signal applied.

$$E(t) = \frac{k_0}{c_0}\ 0.5\ e^{0.5\ t_{mix}{}^{-2}\sigma^2 - t_{mix}{}^{-1}(t-t_{ds})}\ \mathrm{erfc}\left(\frac{t_{mix}{}^{-1}\sigma^2 - (t-t_{ds})}{\sqrt{2}\sigma}\right) \tag{5}$$

For PRMG, a correlation to the SFL for the dimensionless form of these characteristic model parameters considering the rotation speed (Eq. (6), (7) and (8)) has been identified, which follows a Power-approach (Lang et al., 2023).

$$t_{ds}^{*} = t_{ds}\ n \tag{6}$$

$$\sigma^{*} = \sigma\ n \tag{7}$$

$$t_{mix}^{*} = t_{mix}\ n \tag{8}$$

3. Results and discussion

3.1. Impact on general transport function of PRMG

Suitable indicators for the process parameter effect on the residence time are the median of the distribution (t_{50}) or the mean residence time ($\bar{t}$) (Table 1). For the executed experimental investigations, the impact of the parameter variations is the same for both. This is expected with respect to their mathematical definition (Eq. (3) and (4)). Hereby, the values of $\bar{t}$ are shifted to larger values due to the general positive skewness of the RTD profile for screw

Table 1
Overview on specific feed load, determined median of the residence time distribution and mean residence time at each set point in dependency of the module configuration. Parameter set marked with * could not be executed experimentally due to a restriction of the motor torque.

$\dot{m}_{set}$ (kg h^{-1})	n_{set} (min^{-1})	*SFL* (–)			t_{50} (s)			$\bar{t}$ (s)		
		3 SSP	5 SSP	7 SSP	3 SSP	5 SSP	7 SSP	3 SSP	5 SSP	7 SSP
0.3	60	0,0047	0,0061	0,0081	255	331	284	283	367	298
0.3	120	0,0024	0,0030	0,0042	254	282	241	289	329	263
0.3	180	0,0016	0,0020	0,0028	215	285	222	241	323	245
0.3	240	0,0012	0,0015	0,0021	185	266	192	218	296	214
0.6	60	0,0093	0,0118	0,0166	169	194	167	191	218	186
0.6	120	0,0047	0,0060	0,0083	134	174	153	163	203	175
0.6	180	0,0031	0,0040	0,0055	131	143	136	161	168	150
0.6	240	0,0023	0,0030	0,0042	125	140	137	155	163	152
0.9	60	0,0141	0,0180	0,0233	135	132	120	157	156	133
0.9	120	0,0069	0,0090	0,0126	113	117	115	135	141	128
0.9	180	0,0047	0,0061	0,0084	102	118	105	128	141	116
0.9	240	0,0035	0,0045	0,0063	104	106	111	131	128	125
1.2	60	0,0180	0,0239	*	125	127	*	146	149	0
1.2	120	0,0093	0,0119	0,0165	98	115	91	122	138	103
1.2	180	0,0062	0,0082	0,0110	90	100	85	114	122	92
1.2	240	0,0046	0,0060	0,0083	91	92	89	121	109	102

machines (Wesholowski, Podhaisky, & Thommes, 2019). For a constant module configuration, an increase of the feed rate ($\dot{m}$) respectively of the rotation speed (n) result in a shift of the RTD to shorter exit times. This is in agreement to the findings presented in (Lang et al., 2023) for PRMG. The shift of the residence time in these cases has been addressed to a change of the fill level. For higher throughputs at a constant rotation speed, the fill level increases, but proportionally lower. Therefore, the mean transport velocity increases. For higher rotation speeds at a constant feed rate, the applied shear energy increases leading to a reduction of the accumulated material in the granulator and consequently of the transportation time.

In comparison, the effect of the free process volume is not as clear and has to be evaluated in more detail. The highest residence times are typically connected to the medium level of planetary spindles, while the assignment of the lowest residence times varies from the lowest number of planetary spindles (0.3, 0.6, 0.9 kg h^{-1}) to the highest number of planetary spindles for the highest feed rate applied. This varying effect of the free process volume indicates an alteration of the residence time distribution in more than one way, which is illustrated by the determined RTDs for a representative parameter set (Fig. 2).

A reduction of the free process volume by a shift from three (green) to five (orange) planetary spindles leads to a shift to higher exit times, while the profile itself seems to remain rather unchanged with respect to the peak height and relative width. In contrast, a further reduction of the free process volume by seven (blue) planetary spindles results in a narrower RTD symbolized by a higher peak. At the same time, the on-set is not affected and the off-set appears earlier in time. Consequently, the median is located at shorter exit times (Table 1). Overall, the free process volume influences the transportation function and for a reduction the results indicate hereby a shift towards plug flow.

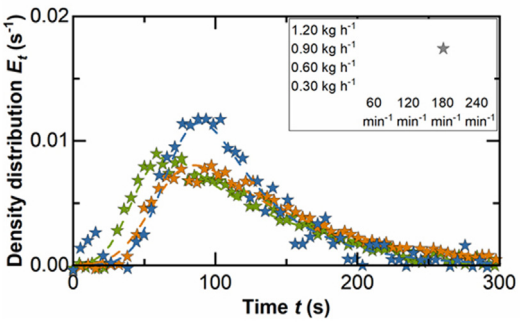

Fig. 2. Determined residence time distribution for a number of three (green), five (orange) and seven (blue) planetary spindles within the module at a representative process parameter set within the experimental design space (Table 1). Symbols represent experimental data; lines represent fitted Two-Compartment-model.

However, in all cases the experimental data (symbols) are represented sufficiently by the Two-Compartment model. Therefore, a further evaluation of the fitted data is suitable to substantiate the insights on the process volume impact on the RTD. A sufficient approach in this context is to utilize the normalized residence time density function ($E\,\bar{t}$), since here the time domain is relativized by the mean residence time ($\Theta = t\,\bar{t}^{-1}$). This data transformation is considered in reverse for the probability values as well. Thereby, a scaling of the density distribution by the time is faded out, which allows a comparison of the fundamental residence time profile respectively transportation function (Fig. 3).

The residence time profiles at each constant rotation speed are ordered in classes according to the free process volume represented by the colors for the different feed rates. This implies a minor impact of the varied feed rate on the transportation characteristic in comparison to the other investigated factors. Hereby, an increase of the screw speed leads in general to wider normalized RTDs. This can be addressed to the higher applied shear energy and number of mixing events. Thereby, the group for seven planetary spindles (blue) is always connected to the narrowest distributions with the highest peak. In contrast, the other two groups overlap and represent a wider distribution with a lower peak. Consequently, the minimization of the free process volume must have an influence on the fundamental transportation mechanisms of PRMG in order to lead to a shift of the resulting transportation function. A detailed analysis of this correlation is feasible via the evaluation of the characteristic parameters of the fitted RTD-model.

3.2. Impact on axial transport during PRMG

According to the applied Two-Compartment-model for the RTD data representation, the axial material transport is symbolized by the dead time respectively the width (Table 2).

In general, the dimensionless duration of axial transport (Fig. 4, top) and the corresponding width (Fig. 4, bottom) follow an exponential decay for larger feed loads at a constant module

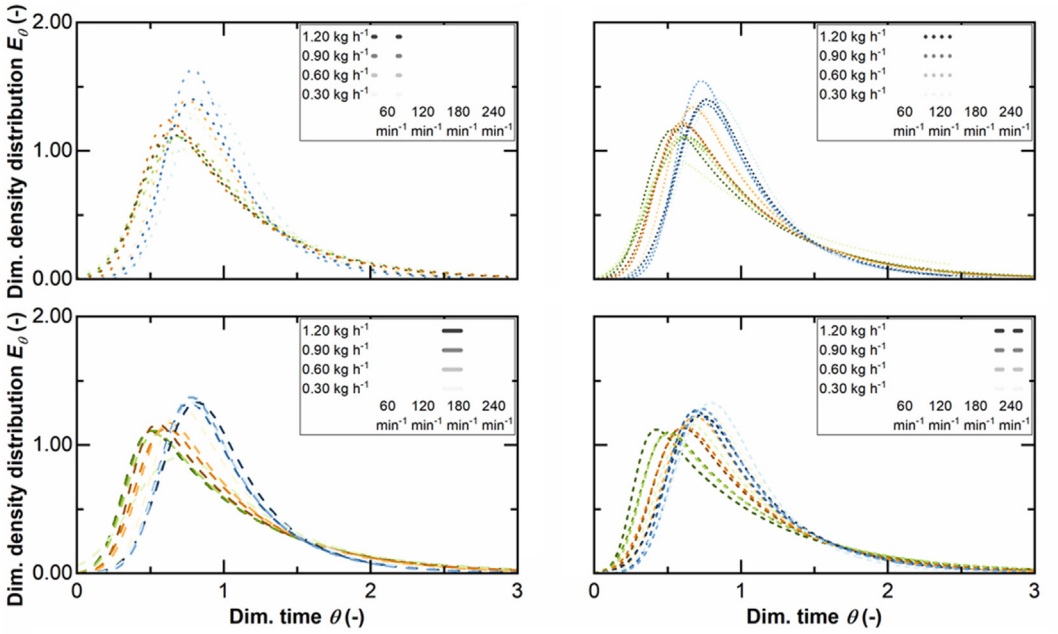

Fig. 3. Normalized residence time density distribution for the fitted Two-Compartment model to the experimental data sets. Colors encode for three (green), five (orange) and seven (blue) planetary spindles within the module, color saturation for the feed rate and line type for the rotation speed within the experimental design space (Table 1).

Table 2
Overview on determined characteristic parameters for the fit of the Two-Compartment-model to the experimental data for each set point in dependency of the module configuration. Parameter set marked with * could not be executed experimentally due to a restriction of the motor torque.

$\dot{m}_{set}$ (kg h^{-1})	n_{set} (min^{-1})	t_{DS} (s)			σ (s)			t_{mix} (s)		
		3 SSP	5 SSP	7 SSP	3 SSP	5 SSP	7 SSP	3 SSP	5 SSP	7 SSP
0.3	60	136	206	213	62.1	56.9	56.4	157	172	95.8
0.3	120	95.7	168	168	42.0	42.6	47.8	249	159	91.5
0.3	180	104	171	145	59.0	47.3	40.6	143	155	102
0.3	240	100	169	130	33.3	51.3	40.9	118	127	78.4
0.6	60	94.7	126	118	36.9	34.0	26.1	97.5	88.5	61.7
0.6	120	64.6	102	101	25.9	26.0	21.7	96.6	100	69.9
0.6	180	55.3	73.9	90.8	20.7	23.9	23.9	108	93.0	58.4
0.6	240	50.7	80.9	84.3	17.3	25.2	22.3	108	79.6	69.5
0.9	60	72.8	69.9	81.7	29.6	19.8	21.6	82.6	86.7	49.7
0.9	120	56.2	60.0	75.2	23.1	17.3	19.1	75.7	79.7	53.4
0.9	180	42.6	58.1	68.3	15.7	19.9	18.7	83.8	82.7	47.0
0.9	240	42.7	53.6	64.0	16.0	19.1	16.9	87.7	72.3	62.6
1.2	60	65.3	68.8	*	24.2	24.5	*	82.0	77.7	*
1.2	120	44.1	58.6	60.7	15.0	18.9	16.8	75.9	77.3	40.0
1.2	180	37.1	45.7	58.0	14.0	14.1	17.2	75.9	75.7	34.6
1.2	240	32.5	45.0	53.4	11.1	14.8	17.9	86.0	63.4	47.7

configuration. This is in agreement with a previous study, where the fill level inside the machine was identified as origin for the described correlation balancing the applied shear force to the material and the transport resistance based on the material velocity (Lang et al., 2023). Therefore, an increase of the feed rate at a constant rotation speed results in an enhanced transportation velocity as the corresponding increase of the fill level is proportionally lower. Consequently, t_{ds} and σ (Table 2) as well as t_{DS}^* and σ^* (Fig. 4) are reduced. At the same time, a decrease of the rotation speed at a constant feed rate results in a proportionally lower increase of the fill level. Therefore, t_{ds} and σ increase as the transport velocity is lower, while t_{DS}^* and σ^* decrease due to the consideration of the rotation speed within the dimensionless form of these parameters.

In addition, an increase of the applied planetary spindles per module leads for constant direct process parameters to a longer lasting axial transport of the material during processing (Table 2) and therefore higher values for the dimensionless parameters at a constant feed load in comparison (Fig. 4, top). This is counter-intuitive in the first moment as the reduction of the free process volume and the enhanced number of shearing events should overall lead to a higher transport velocity. The first aspect is reflected per definition in the SFL, while the second aspect is not addressed so far. Here, a suitable surrogate is the created contact surface ($S_{contact}$) by the rotation of the planetary spindles. This needs to be related to the overall inner surface (S_{inner}) within the processing section for an overarching approach with respect to the machine size (Eq. (9)).

$$f_S = \frac{\pi\, d_{PS}\, l_{CS}\, N_{PS}}{\pi\,(d_{RC} + d_{CS})\, l_{CS}} \tag{9}$$

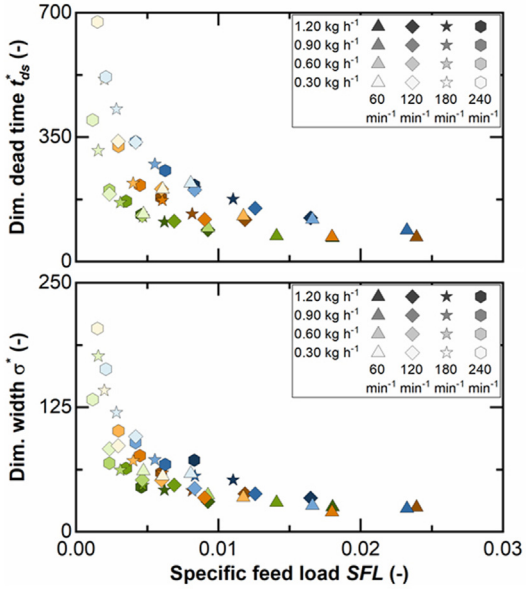

Fig. 4. Dimensionless dead time (top) and width (bottom) of the fitted Two-Compartment model to the experimental data sets. Colors encode for three (green), five (orange) and seven (blue) planetary spindles within the module, color saturation for the feed rate and symbol type for the rotation speed within the experimental design space (Table 1).

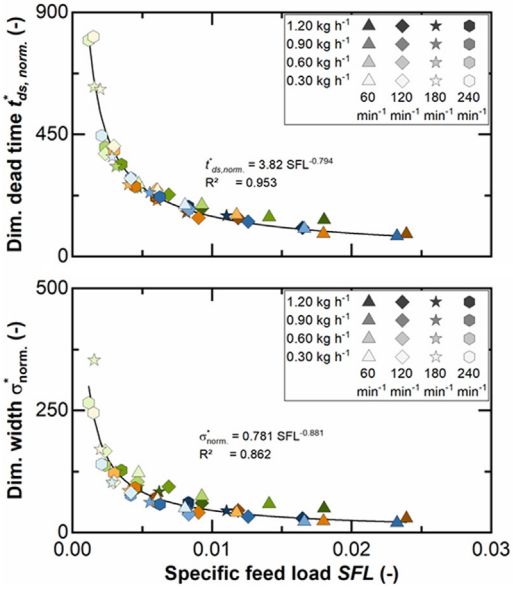

Fig. 5. Normalized, dimensionless dead time (top) and width (bottom) of the fitted Two-Compartment model to the experimental data sets. Colors encode for three (green), five (orange) and seven (blue) planetary spindles within the module, color saturation for the feed rate and symbol type for the rotation speed within the experimental design space (Table 1).

$$t^*_{ds,norm.} = \frac{t^*_{ds}}{f_S} \tag{10}$$

$$\sigma^*_{norm.} = \frac{\sigma^*}{f_S} \tag{11}$$

The correction factor (f_S) for the contact surface depends on the number (N_{PS}) and diameter (d_{PS}) of these in comparison to the diameter of the roller cylinder (d_{RC}) and the central spindle (d_{CS}). This ratio is constant for the processing section length (l_{CS}) and applied to normalize the dimensionless parameters (Eqs. (10) and (11)).

The normalized dimensionless parameters of the Two-Compartment model related to the axial material transport coincide to a master curve for each case individually (Fig. 5). This indicates a fundamental transport mechanism, which is indeed related to the contacted surface by the rotation of the planetary spindle. However, in this context the impact of an individual element must be constant. Otherwise, the variation of the spindle number could not be balanced by the correction factor. Furthermore, the overall sufficient correlation of the normalized parameters to the SFL following a power approach imply the relevance of the fill level with respect to the transport mechanism as well. Thereby, the coefficient of determination are categorized as sufficient with respect to an experimental determination and the covered design space. The lower value in comparison for the dimensionless width can be addressed to the setting of on-and off-set, which is naturally more subject to fluctuations as the location of the peak location instead.

3.3. Impact on material mixing during PRMG

According to the applied Two-Compartment-model for the RTD data representation, the mixing time refers to the blending of the material during processing (Table 2). In general, the dimensionless mixing duration follows an exponential decay for larger feed loads at a constant module configuration (Fig. 6). This refers to the applied shear rate in relation to the fill level inside the apparatus and is in agreement with previous studies (Lang et al., 2023). For a constant rotation speed, the increase of the feed rate leads to an accumulation of material in the granulator (Lang et al., 2023) and an overall reduction of the median residence time (Table 1). In combination with a constant shear rate, this results in less mixing of more material. For a constant feed rate, a decrease of the rotation speed leads to a diminished shear stress applied and an enhanced fill level. Consequently, more material inside is mixed less.

At the same time, a clear visual deviation between the different module configurations is hardly feasible as the individual values of the different configurations overlap. In contrast, the non-transformed values (Table 2) allow a categorization according to the applied number of planetary spindles in two groups as only the values for the lowest free processing volume are significantly lower ($\alpha = 0.01$) in comparison to the configuration with the highest free

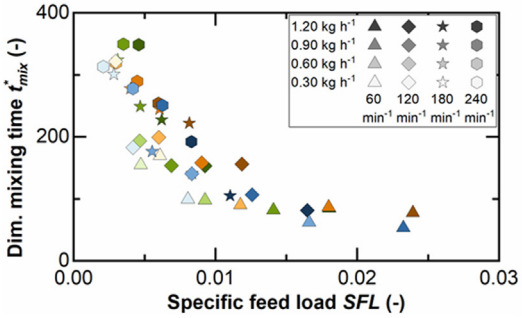

Fig. 6. Normalized, dimensionless dead time (top) and width (bottom) of the fitted Two-Compartment model to the experimental data sets. Colors encode for three (green), five (orange) and seven (blue) planetary spindles within the module, color saturation for the feed rate and symbol type for the rotation speed within the experimental design space (Table 1).

processing volume. This is in agreement with the findings concerning the impact on the RTD profile in general and the differentiation of two classes, where the configurations with three and five planetary spindles form one and seven planetary spindles the other one.

Consequently, the dimensionless approach has to be complemented in order to normalize the data with respect to the module configuration. As the mixing time refers to the overall mixing volume according to the model theory (Reitz et al., 2013), the applied approach extension (Eq. (12)) considers a surrogate for the relative fill level ($t_{50}\ \tau^{-1}$) referring to (Lang et al., 2023) as well as the free-processing area related to the inner cross-sectional area of the roller cylinder (A_{RC}). This reflects mathematically the filled-up material inside relative to the machine size. Here, the theoretical maximum transport time (τ) symbolizes an idealized material transport with no backmixing in a fully filled machine (Eq. (13)).

$$t^*_{mix,norm.} = t^*_{mix} \left(\frac{t_{50}}{\tau} \frac{A_{free}}{A_{RC}} \right)^{-1} \tag{12}$$

$$\tau = \left(SFL\ n\ \frac{l_{CS}}{h_{CS}} \right)^{-1} \tag{13}$$

The normalized dimensionless mixing time of the Two-Compartment model coincide for the different module configurations to a master curve (Fig. 7) with an overall coefficient of determination beyond 0.95 for the fit to a power approach. This indicates a fundamental mixing mechanism, which is indeed related to the material inside the granulator during processing as well as the rotation of the planetary spindles and the specific feed load.

4. Conclusion

The variation of the free process volume via the spindle configuration of the processing section is a suitable tool to modulate the material transport during planetary roller melt granulation. The normalization of the fitted residence time functions highlight a lower impact of the feed rate on the underlying transport function in comparison to the rotation speed or free processing volume. Thereby, an increase of the rotation speed leads to a wider residence time distribution enhancing the material mixing, while a higher planetary spindle number leads to a characteristic shift towards a narrower residence distribution connected to plug flow. Furthermore, the results in terms of the experimentally determined residence times and the applied model are in general in a good agreement to the previous investigations. The normalization of the data concerning the characteristic RTD model parameters demonstrated the need to differentiate two aspects regarding the fundamental transport mechanism. While the axial transport is apparently connected to the generated contact area, the mixing extend depends on the actual material inside the granulator. Hereby, both mechanisms also seem to be directly related to the rotation speed.

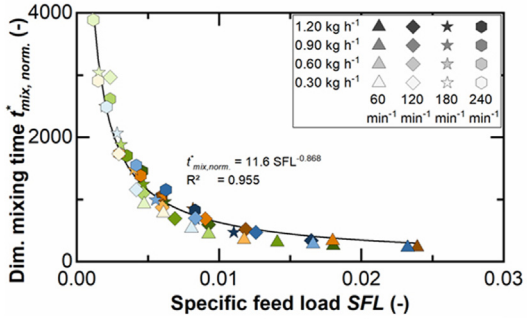

Fig. 7. Normalized, dimensionless mixing time of the fitted Two-Compartment model to the experimental data sets. Colors encode for three (green), five (orange) and seven (blue) planetary spindles within the module, color saturation for the feed rate and symbol type for the rotation speed within the experimental design space (Table 1).

Declaration of competing interest

The authors declare that they have no known competing financial interests or personal relationships that could have appeared to influence the work reported in this paper.

Acknowledgments

The authors would like to thank Entex Rust & Mitschke GmbH (Bochum, Germany) for the opportunity to conduct the experiments with the planetary roller granulator and MeltPrep GmbH (Graz, Austria) for the opportunity to execute the residence time determination with the ExtruVis system. The authors also like to thank Merck Healthcare KGaA (Darmstadt, Germany) for providing lactose as model compound and Ashland Industries Deutschland GmbH (Düsseldorf, Germany) for providing the melt binder used in the melt granulation studies.

References

Aldhafeeri, T., Alotaibi, M., & Barry, C. F. (2022). Impact of melt processing conditions on the degradation of Polylactic Acid. *Polymers, 14*(14), Article 2790. https://doi.org/10.3390/polym14142790

Bhalode, P., Tian, H. Y., Gupta, S., Razavi, S. M., Roman-Ospino, A., Talebian, S., … Ierapetritou, M. (2021). Using residence time distribution in pharmaceutical solid dose manufacturing-A critical review. *International Journal of Pharmaceutics, 610*, Article 121248. https://doi.org/10.1016/j.ijpharm.2021.121248

Ellwanger, F., Pernice, L., Karbstein, H. P., & Emin, M. A. (2023). Investigating local residence time and thermomechanical stress profile in twin-screw extrusion of plant proteins by using the moving particle semi-implicit simulation method. *Journal of Food Engineering, 359*, Article 111665. https://doi.org/10.1016/j.jfoodeng.2023.111665

Forgber, T., Rehrl, J., Matic, M., Sibanc, R., Sivanesapillai, R., & Khinast, J. G. (2022). Experimental and numerical investigations of the RTD in a GEA ConsiGma CTL25 tablet press. *Powder Technology, 405*, Article 117507. https://doi.org/10.1016/j.powtec.2022.117507

Forster, S. P., Dippold, E., & Chiang, T. Y. (2021). Twin-screw melt granulation for oral solid pharmaceutical products. *Pharmaceutics, 13*(5), Article 665. https://doi.org/10.3390/pharmaceutics13050665

Forster, S. P., Dippold, E., Haser, A., Emanuele, D., & Meier, R. (2023). Integrated continuous wet granulation and Drying: Process evaluation and comparison with Batch processing. *Pharmaceutics, 15*(9), Article 2317. https://doi.org/10.3390/pharmaceutics15092317

Gottschalk, T., Grönniger, B., Ludwig, E., Wolbert, F., Feuerbach, T., Sadowski, G., et al. (2022). Influence of process temperature and residence time on the manufacturing of amorphous solid dispersions in hot melt extrusion. *Pharmaceutical Development and Technology, 27*(3), 313–318. https://doi.org/10.1080/10837450.2022.2051549

Gyürkés, M., Madarász, L., Köte, A., Domokos, A., Mészáros, D., Beke, A. K., … Farkas, A. (2020). Process design of continuous powder blending using residence time distribution and feeding models. *Pharmaceutics, 12*(11), Article 1119. https://doi.org/10.3390/pharmaceutics12111119

ICH. (2023). *Continuous manufacturing of drug substances and drug products Q13*.

Iveson, S. M., Litster, J. D., Hapgood, K., & Ennis, B. J. (2001). Nucleation, growth and breakage phenomena in agitated wet granulation processes: A review. *Powder Technology, 117*(1–2), 3–39. https://doi.org/10.1016/S0032-5910(01)00313-8

Karttunen, A. P., Hörmann, T. R., De Leersnyder, F., Ketolainen, J., De Beer, T., Hsiao, W. K., et al. (2019). Measurement of residence time distributions and material tracking on three continuous manufacturing lines. *International Journal of Pharmaceutics, 563*, 184–197. https://doi.org/10.1016/j.ijpharm.2019.03.058

Kleinebudde, P., Khinast, J., & Rantanen, J. (2017). *Continuous manufacturing of pharmaceuticals* (1st ed.).

Kohlgrüber, K. (2016). *Der gleichläufige Doppelschneckenextruder - Grundlagen, technologie, Anwendungen*. München: Carl-Hanser-Verlag.

Lang, T. M., Bramböck, A., Thommes, M., & Bartsch, J. (2023). Material transport characteristics in planetary roller melt granulation. *Pharmaceutics, 15*(8), Article 2039. https://doi.org/10.3390/pharmaceutics15082039

Liu, T. Z., & Zhang, F. (2023). Modelling drug degradation of amorphous solid dispersion during twin-screw extrusion. *European Journal of Pharmaceutics and Biopharmaceutics, 190*, 197–205. https://doi.org/10.1016/j.ejpb.2023.07.020

Nesges, D., Lang, T. M., Birr, T., Thommes, M., & Bartsch, J. (2023). Planetary roller melt granulation (PRMG)-A new continuous method for powder processing. *Powder Technology, 427*, Article 118728. https://doi.org/10.1016/j.powtec.2023.118728

Pauli, V., Kleinebudde, P., & Krumme, M. (2020). From powder to tablets: Investigation of residence time distributions in a continuous manufacturing process train as basis for continuous process verification. *European Journal of Pharmaceutics and Biopharmaceutics, 153*, 200–210. https://doi.org/10.1016/j.ejpb.2020.05.030

Peterwitz, M., Gerling, S., & Schembecker, G. (2022). Challenges in tracing material flow passing a loss-in-weight feeder in continuous manufacturing processes. *International Journal of Pharmaceutics, 612*, Article 121304. https://doi.org/10.1016/j.ijpharm.2021.121304

Plath, T., Korte, C., Sivanesapillai, R., & Weinhart, T. (2021). Parametric study of residence time distributions and granulation Kinetics as a basis for process modeling of twin-screw wet granulation. *Pharmaceutics, 13*(5), Article 645. https://doi.org/10.3390/pharmaceutics13050645

Pradhan, A., Costello, M., Yang, F. Y., Bi, V. V., Durig, T., & Zhang, F. (2022). Using twin-screw melt granulation to co-process mannitol and hydroxypropylcellulose. *Journal of Drug Delivery Science and Technology, 77*, Article 103880. https://doi.org/10.1016/j.jddst.2022.103880

Puckhaber, D., Eichler, S., Kwade, A., & Finke, J. H. (2020). Impact of particle and equipment properties on residence time distribution of pharmaceutical Excipients in rotary tablet Presses. *Pharmaceutics, 12*(3), Article 283. https://doi.org/10.3390/pharmaceutics12030283

Razavi, S. M., Román-Ospino, A. D., Bhalode, P., Scicolone, J., Callegari, G., Dubey, A., … Muzzio, F. (2023). Selection of an appropriate tracer to measure the residence time distribution (RTD) of continuous powder blending operations. *Powder Technology, 429*, Article 118864. https://doi.org/10.1016/j.powtec.2023.118864

Reitz, E., Podhaisky, H., Ely, D., & Thommes, M. (2013). Residence time modeling of hot melt extrusion processes. *European Journal of Pharmaceutics and Biopharmaceutics, 85*(3), 1200–1205. https://doi.org/10.1016/j.ejpb.2013.07.019

Rosas, J. G., Brush, P., Thompson, B., Miller, C., Overton, P., Tugby, N., … Conway, S. L. (2023). Implementation of a fully integrated CM direct compression and coating process at a commercial pharmaceutical facility-Part 2: PAT and RTD results for normal operational conditions batches. *International Journal of Pharmaceutics, 636*, Article 122814. https://doi.org/10.1016/j.ijpharm.2023.122814

Sekyi, N. K. G., Kelly, A., & Rahmanian, N. (2023). Comparative analysis of granule properties in continuous granulators. *Powder Technology, 425*, Article 118557. https://doi.org/10.1016/j.powtec.2023.118557

Serno, P., Kleinebudde, P., & Knop, K. (2007). *Granulieren: Grundlagen, Verfahren, Formulierungen: ECV - Editio-Cantor-Verlag*.

Sibanc, R., Turk, M., & Dreu, R. (2018). An analysis of the mini-tablet fluidized bed coating process. *Chemical Engineering Research and Design, 134*, 15–25. https://doi.org/10.1016/j.cherd.2018.03.020

Tian, H. Y., Bhalode, P., Razavi, S. M., Koolivand, A., Muzzio, F. J., & Ierapetritou, M. G. (2022). Characterization and propagation of RTD uncertainty for continuous powder blending processes. *International Journal of Pharmaceutics, 628*, Article 122326. https://doi.org/10.1016/j.ijpharm.2022.122326

Tomita, Y., Takeuchi, Y., Natsuyama, S., & Takeuchi, H. (2021). Characteristics of residence time distribution in a continuous high shear mixer granulation using scraper rotation. *International Journal of Pharmaceutics, 605*, Article 120789. https://doi.org/10.1016/j.ijpharm.2021.120789

van de Steene, S., Van Renterghem, J., Vanhoorne, V., Vervaet, C., Kumar, A., & De Beer, T. (2023a). Elucidation of granulation mechanisms along the length of the barrel in continuous twin-screw melt granulation. *International Journal of Pharmaceutics, 639*, Article 122986. https://doi.org/10.1016/j.ijpharm.2023.122986

van de Steene, S., Van Renterghem, J., Vanhoorne, V., Vervaet, C., Kumar, A., & De Beer, T. (2023b). Visualization of the granule temperature using thermal imaging to improve understanding of the granulation mechanism in continuous twin-screw melt granulation. *International Journal of Pharmaceutics, 645*, Article 123423. https://doi.org/10.1016/j.ijpharm.2023.123423

Van Renterghem, J., Kumar, A., Vervaet, C., Remon, J. P., Nopens, I., Vander Heyden, Y., et al. (2017). Elucidation and visualization of solid-state transformation and mixing in a pharmaceutical mini hot melt extrusion process using in-line Raman spectroscopy. *International Journal of Pharmaceutics, 517*(1–2), 119–127. https://doi.org/10.1016/j.ijpharm.2016.11.065

Weatherley, S., Mu, B. O., Thompson, M. R., Sheskey, P. J., & O'Donnell, K. P. (2013). Hot-melt granulation in a twin screw extruder: Effects of processing on Formulations with Caffeine and Ibuprofen. *Journal of Pharmaceutical Sciences, 102*(12), 4330–4336. https://doi.org/10.1002/jps.23739

Wesholowski, J., Hoppe, K., Nickel, K., Muehlenfeld, C., & Thommes, M. (2019). Scale-Up of pharmaceutical Hot-Melt-Extrusion: Process optimization and transfer. *European Journal of Pharmaceutics and Biopharmaceutics, 142*, 396–404. https://doi.org/10.1016/j.ejpb.2019.07.009

Wesholowski, J., Podhaisky, H., & Thommes, M. (2019). Comparison of residence time models for pharmaceutical twin-screw-extrusion processes. *Powder Technology, 341*, 85–93. https://doi.org/10.1016/j.powtec.2018.02.054

Wilms, A., & Kleinebudde, P. (2021). Optimization of residence time distribution in RCDG and an assessment of its applicability in continuous manufacturing. *Particuology, 56*, 43–49. https://doi.org/10.1016/j.partic.2020.09.009

Winck, J., Daalmann, M., Berghaus, A., & Thommes, M. (2022). In-line monitoring of solid dispersion preparation in small scale extrusion based on UV-vis spectroscopy. *Pharmaceutical Development and Technology, 27*(10), 1009–1015. https://doi.org/10.1080/10837450.2022.2144887

Yaghini, N., & den Doelder, J. (2023). Simulations mapping the influence of oxygen, extruder residence time, and mechanical shear on low-density polyethylene structure during recycling. *Polymer, 265*, Article 125596. https://doi.org/10.1016/j.polymer.2022.125596